Electrochemistry of uranium in molten LiCl-LiF

Sylvain Geran, Pierre Chamelot, Jérome Serp, Mathieu Gibilaro, Laurent Massot

Electrochemistry of uranium in molten LiCl-LiF

S. Geran[a,b], P. Chamelot[b,*], J. Serp[a], M. Gibilaro[b], L. Massot[b]

[a] Nuclear Energy Division, RadioChemistry & Processes Department, CEA Marcoule, Bagnols-sur-Cèze 30207, France
[b] Laboratoire de Génie Chimique, Université de Toulouse, CNRS, INPT, UPS, Toulouse, France

Keywords:
Molten chloro-fluoride media
Electrochemistry
Uranium
Fluoride stabilizing effect
Electrochemical reaction mechanism

A B S T R A C T

This work is focused on the electrochemical behaviour of uranium in molten eutectic LiCl–LiF (70–30 mol%) in the 550–650 °C temperature range. On tungsten electrode, U(III) ions were reduced in one step to U metal exchanging 3 electrons and oxidized also in one step to U(IV) exchanging one electron. Both systems were studied by cyclic and square wave voltammetries and chronopotentiometry. The reduction and oxidation mechanisms of U(III) ions were found to be diffusion controlled processes. The diffusion coefficient of U(III) was measured at different temperatures, and it followed an Arrhenius "type law". Apparent standard potentials were measured in chloride-fluoride (LiCl-LiF eutectic) and pure chloride media (LiC-KCl eutectic). The addition of fluoride ions into a chloride salt leads to the formation of more stable complexes reduced at more negative potentials. This shift of reduction potentials is more pronounced for the U(IV)/U(III) transition (~500 mV) than for the U(III)/U system (~100 mV).

1. Introduction

Molten salts are studied in the nuclear industry because of their resistance to radiolysis and their large electrochemical window allowing the production of actinide metals. Chloride salts, and particularly the LiCl-KCl eutectic, has been proposed and used in semi industrial scale as solvent for the treatment of U-Zr and U-Pu-Zr irradiated metallic fuels by electro-refining [1–3]. In this electrolytic process, actinides and fission products (mainly alkali metals and lanthanides) are anodically dissolved in the molten salt while pure uranium metal can be collected on inert cathode [4]. The group recovery of actinides, i.e. U together with transuranium elements (Pu, Np, Am, Ac, Cm), is limited on inert cathode by the chemical reactions between U(III) ions dissolved in the molten salt phase and deposited transuranium elements (TRU's) [5–8]:

$$U(III) + TRU = TRU(III) + U \quad (1)$$

Liquid cadmium cathodes were therefore developed for the recovery of TRU(s) [9–11] by solubilizing the TRU(s) into liquid Cd trough the formation of stable alloys. Other reactive cathode materials such as bismuth [12], aluminum [13] and gallium [14,15] were proven suitable for homogeneous recovery of all actinides as alloys. The use of reactive cathodes, however, requires an additional step to obtain actinide for new fuel fabrication. For example, the actinide/cadmium separation step is carried out by distillation under reduced pressure. In the case of U-Pu-Cd alloys, Cd concentration in the final product is below 100 ppm [16]. However, the lanthanides/actinides separation factor on these reactive cathodes is lower than on an inert solid cathode [17].

Fluoride salts application in the nuclear field are numerous, from the metallic uranium production by reduction of UF_4 green salt [18] or by electrolysis of uranium oxides [19], to the development of molten salt reactors [20,21] and separation processes for clean-up of the MSR fuel salt and for recovery of actinides from spent nuclear fuel by different pyrochemical processes including-fluoride volatility process [22]. In comparison to chloride salts, fluoride solvents limit the number of species oxidation states as reported for instance by Lambertin et al. [23] for the americium case. The results obtained by Quaranta et al. [24] and Sakamura et al. [25] on Zr(IV) electrochemical reduction in LiF-NaF and LiCl-KCl also illustrate the difference between chloride and fluoride solvent in terms of complexation: in LiF-NaF, a single transition from Zr(IV) to Zr is obtained, whereas Zr(IV), Zr(II) and Zr(I) are observed in LiCl-KCl. Limiting the number of stable oxidation states helps the quantitative recovery of metals by molten salt electrolysis as showed for neodymium and dysprosium by Diaz et al. [26].

The uranium systems have been studied in both chloride and fluoride media.

In molten chloride salt, uranium ions electrochemical behavior was studied by Serrano et al. between 973 K and 988 K in NaCl-KCl [27], and in LiCl-KCl by various authors [28–34]. The U(III) ions are reduced in one step, exchanging 3 electrons, to U and oxidized to

* Corresponding author.
E-mail address: chamelot@chimie.ups-tlse.fr (P. Chamelot).

https://doi.org/10.1016/j.electacta.2020.136784

U(IV) in one step exchanging 1 electron. Both systems were found reversible and diffusion controlled.

In molten LiF-CaF_2, uranium ions were studied by Hamel et al. [35] and Nourry et al. [36] at 1083 K. The reduction of U(IV) proceeds via two steps exchanging 1 and 3 electrons, leading to the formation of uranium metal. Both systems are found to be diffusion controlled.

The influence of fluoride addition to chloride salt on the reduction mechanism of various metals (e.g. Zr, Ti, Hf, Nb, Ta, Nd) has been frequently reported to improve the electrolytic recovery yields. In these studies, the molar ratio between fluoride ions and the metal ions to be plated in molten chloride is usually low. Studies devoted to mixed chloro-fluoride salts are scarce, plating iron in $CaCl_2$–CaF_2 was reported by Haarberg and al. [37] and, more recently, Ti electrodeposition in both LiCl-LiF and water soluble KCl-KF has been investigated [38].

In this work, the chloro-fluoride salts were considered as a potential solvent for recycling the nuclear metallic fuel. They combine the stabilizing effects of fluoride ions, which usually simplify the reduction mechanisms, and the presence of chloride ions that allow the production of chlorine gas in electrolytic conditions of oxygen free medium. This type of salts would make the electrolytic recovery of americium more efficient by limiting the existence of Am(II) species as shown for neodymium and dysprosium [39], both having superior recovery rates and faradic yields in LiCl-LiF than in LiCl-KCl. The chloro-fluorinated mixture chosen is LiCl-LiF and the actinide studied in this work is uranium as there are no available published data in this field.

2. Experimental

2.1. Electrochemical experiment

The experiments on uranium in LiCl-LiF were performed in a glove box under air atmosphere. The cell consisted of a vitreous carbon crucible placed in a quartz counter crucible to prevent molten salt from leaking into the quartz cell. The two crucibles were placed in a cylindrical quartz reactor. The reactor was flushed with argon (< 0.1 ppm O_2 and < 0.5 ppm H_2O). The electrochemical experiments were carried out with a three-electrode set up connected to an Autolab potentiostat/galvanostat controlled with Nova 1.11 software. A Mo rod of 3 mm diameter immersed in the salt was used as a comparison electrode (RE). Its potential being dependent on oxide concentration in the melt, chlorine evolution and lithium metal deposition potentials were frequently checked for more accurate measuring. All RE potentials were referred to Cl_2/Cl^- redox couple. the conversion was obtained by graphical estimation of the potential at zero current in the linear variation region during the positive scan of voltammograms as shown in Fig. 1 [38]. The working electrode (WE) was 0.5 mm diameter W wire and the counter electrode (CE) was a 1 mm diameter Mo wire. Cyclic voltammetry, square wave voltammetry (SWV) and chronopotentiometry were used to investigate the electrochemical system.

2.2. Preparation of the melt

Vitreous carbon was selected as material for the crucible. LiCl and LiF (Sigma Aldrich 99.99%) were used for the solvent preparation. The eutectic LiCl-LiF mixture (70–30 mol%) was prepared in the glove box under inert atmosphere ($<$ 10 ppm O_2 and $<$ 10 ppm H_2O) by mixing the pure chemicals. The mixture was heated at 473 K in a reactor flushed with argon (< 0.1 ppm O_2 and < 0.5 ppm H_2O) for 24 h before being melted. The LiCl-KCl eutectics (59–41 mol%) were prepared using pure LiCl and KCl (Sigma Aldrich 99.99%) with the same methodology.

$FeCl_2$ (Sigma Aldrich 99.99%) was added to LiCl-KCl and LiCl-LiF salts and purity of the system was checked by cyclic voltammetry before cool down for salt solidification. The frozen salt was transferred to the air glovebox experiment compatible with uranium experiments. The quick transfer is realized in a sealed container under argon atmosphere. After melting of the salt in the air glovebox, the electrochemical signal of $FeCl_2$ on cyclic voltammogram remained unchanged indicating that no moisture pickup occurred during the transfer.

A molybdenum basket containing uranium metal was lifted down in the salt phase. Uranium(III) ions were produced by chemical oxidation of metallic uranium by Fe(II) ions. The melts were prepared according to reactions (2), (3) and (4) with an excess of U metal:

$$3\,Fe(II) + 2U = 2\,U(III) + 3\,Fe \qquad \Delta G^\circ = -654\ kJ.mol^{-1} \tag{2}$$

$$2\,Fe(II) + U = U(IV) + 2\,Fe \qquad \Delta G^\circ = -306\ kJ.mol^{-1} \tag{3}$$

$$3\,U(IV) + U = 4\,U(III) \qquad \Delta G^\circ = -391\ kJ.mol^{-1} \tag{4}$$

The concentration of uranium species in the bath was determined by X-ray fluorescence analysis of salt samples (~ 0.2 g), dissolved in 10 mL of HNO_3 (4 M).

3. Results and discussion

3.1. Uranium ions reduction mechanism on inert electrode

3.1.1. Cyclic voltammetry

Cyclic voltammograms of pure LiCl-LiF solvent and with addition of U(III) (0.039 mol kg^{-1}) are presented in Fig. 1 on W electrode at 100 mV s^{-1} and 550 °C. Two electrochemical systems are observed: the first soluble-soluble system (I_{red} and I_{ox}) at a potential of –2.0 V vs Cl_2/Cl^- associated to the U(IV)/U(III) couple, and the second one at −2.8 V vs Cl_2/Cl^- with a reduction peak II_{red} and a reoxidation peak II_{ox} associated to the U(III)/U couple. The shape of II_{ox} and II_{red} peaks is characteristic of the electrodeposition of a metal and its dissolution (stripping peak).

The limiting processes of both systems were investigated by plotting the square root of the scan rate versus the peak current density.

For U(III)/U soluble/insoluble system, the reduction peak current density (II_{red}) increases linearly with the square root of the scan rate in the range 10–300 mV s^{-1} as shown in Fig. 2, meaning that the electrochemical reduction of U(III) is controlled by diffusion.

As the value of the peak potential Ep(II_{red}) does not depend on the scan rate (cf. Fig. 2), the reduction process can be considered as reversible. The Berzins-Delahay relationship for the U(III)/U system at the studied working concentration can be applied because of the verified reversibility and soluble-insoluble system [40]:

$$I_p = 0.6102\,n\,FSC^\circ\left(\frac{nF}{RT}\right)^{0.5} D^{0.5}v^{0.5} \tag{5}$$

Where I_p is the peak intensity (A), n the number of exchanged electrons, F the Faraday constant (96,500 C mol^{-1}), C° the solute concentration (mol cm^{-3}), R the gas constant (8.314 $J.mol^{-1}$ K^{-1}), T the temperature (K), D the diffusion coefficient (cm^2 s^{-1}) and v the scan rate (V s^{-1}).

The equation slope for the reduction of U(III) into U reversible system in LiCl-LiF at 550 °C is:

$$\frac{i_{pic}}{v^{0.5}} = -0.32\ A.s^{0.5}.cm^{-2}.V^{0.5} \tag{6}$$

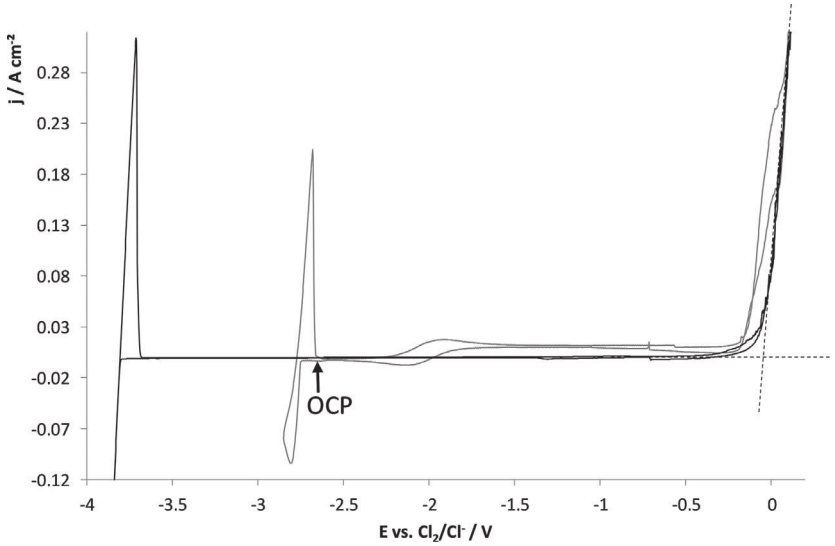

Fig. 1. Cyclic voltammograms on W of the LiCl-LiF system at 100 mV s^{-1} and T = 823 K: pure solvent (black) and with U(III) concentration of 0.039 mol kg^{-1} (grey).

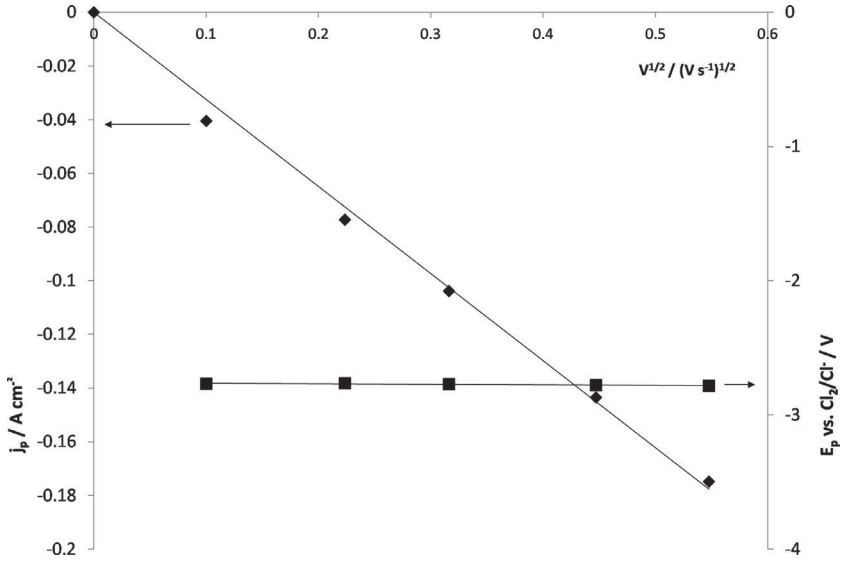

Fig. 2. Variation of the peak current density (left axis) and the reduction peak potential (right axis) vs. the square root of the potential scan rate on W in LiCl-LiF-U(III) (0.039 mol kg^{-1}) system at T = 823 K. Working el.: W; auxiliary el.: Mo; comparison el.: W.

According to Eq. (5), the peak intensity attributed to the reduction of U(III) ions to U metal increases linearly with the concentration of U(III) in the solution. The slope of the calibration curve was found to be -8.6 A.kg.$s^{0.5}$.cm^{-2}.$V^{-0.5}$.mol^{-1} and can be used to determine the U(III) concentration into the solution at 823 K. The U(III) concentration in solution was also verified by X-ray fluorescence after sampling the melt.

The oxidation peak current density (I_{ox}) for U(IV)/U(III) soluble-soluble system increases linearly with the square root of the scan rate in the 50–300 mV s^{-1} range as shown in Fig. 3, showing that U(III) electrochemical oxidation is diffusion controlled. Thus, the Randles–Sevcik relationship for a soluble/soluble system can be used [40]:

$$I_p = 0.446\, n\, FSC^{\circ}\left(\frac{nF}{RT}\right)^{0.5} D^{0.5} v^{0.5} \tag{7}$$

The slope of this equation for the oxidation of U(III) into U(IV) reversible system in LiCl-LiF at 550 °C is:

$$\frac{i_{pic}}{v^{0.5}} = 0.056\,A.s^{0.5}.cm^{-2}.V^{-0.5} \tag{8}$$

The open circuit potential (OCP) on W electrode was -2.65 V vs Cl_2/Cl^-, closed from the U(III)/U system, permitting to conclude that the U(IV) concentration was negligible regarding to U(III) one. It can be also noted that no additional peak was observed on the voltammogramm, showing that presence of Fe(II) is not detected.

3.1.2. Square-wave voltammetry (SWV)

SWV was used to determine the number of exchanged electrons. In the case of a soluble/soluble system, the square wave voltammetry curve has a Gaussian shape. For the soluble/insoluble system the curve obtained is an asymmetric Gaussian due to a nucleation phenomenon [35]. When the linear relationship between the differential peak current density and the square root of the frequency is verified, Eqs. (9) and (10) can be used to calculate the number of exchanged electrons using the width of the peak $W_{1/2}$ at half of the peak height [41,42]:

$$\delta i_p = n\, FC^{\circ}\frac{1-\Omega}{1+\Omega}\left(\frac{Df}{\pi}\right)^{0.5} \quad \text{with} \quad \Omega = \exp\left(\frac{nF\Delta E}{2RT}\right) \tag{9}$$

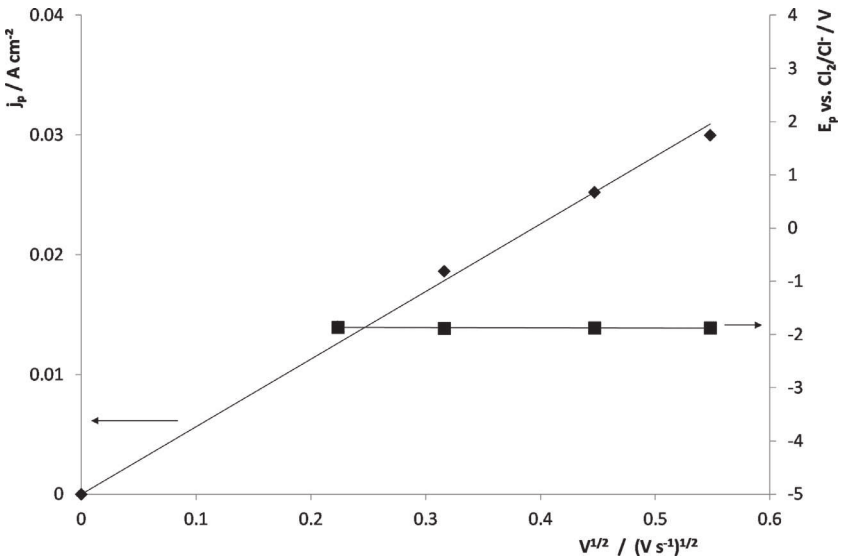

Fig. 3. Variation of the peak current density (left axis) and the oxidation peak potential (right axis) vs. the square root of the potential scan rate on W in LiCl-LiF-U(III) (0.039 mol kg^{-1}) system at T = 823 K. Working el.: W; auxiliary el.: Mo; comparison el.: W.

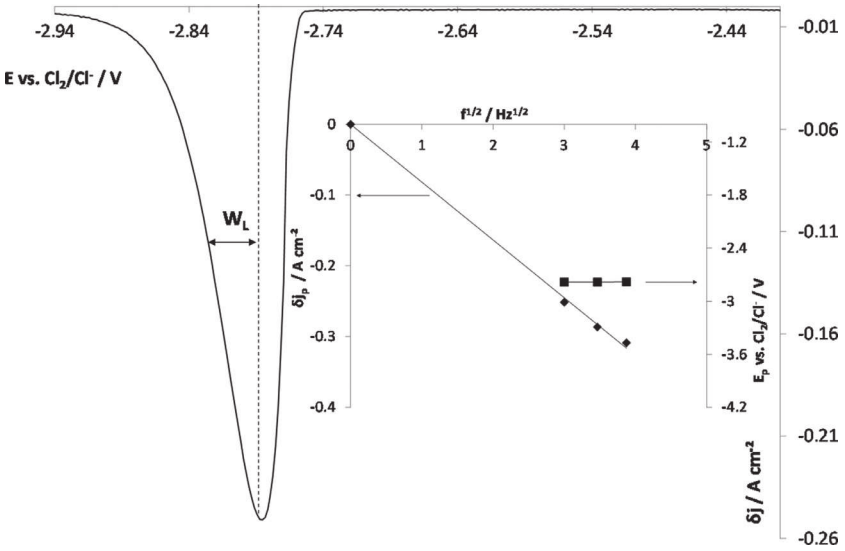

Fig. 4. Square wave voltammogram on W in LiCl-LiF-U(III) (0.06 mol kg^{-1}) system at 9 Hz and T = 823 K. Inset. Variation of the peak current density (left axis) and the reduction peak potential (right axis) vs. the square root of frequency.

$$W_{1/2} = 3.52\frac{RT}{nF} \tag{10}$$

where δi_p is the differential peak current density (A.cm^{-2}), f the frequency (Hz), ΔE the square signal amplitude (V), $W_{1/2}$ the width of the peak at half height of the considered peak (V).

Figs. 4 and 5 show typical square wave voltammograms with the variation of the differential peak current density versus the square root of the frequency for the U(III)/U and U(IV)/U(III) systems. Both voltammograms show a single peak in reduction and oxidation in LiCl-LiF at 550 °C and 9 Hz. This confirms that only U(III) is present in the molten salt (U in excess) and validates the experimental procedure for melt preparation.

The shape of the reduction peak is an asymmetric Gaussian caused by a nucleation overvoltage, leading to a delay in the occurrence of faradic current. This is frequently observed with soluble/insoluble systems involving metal deposition. The validity of Eq. (9) was verified by the linear relationship between the differential peak current density versus the square root of the frequency. The half-width was determined by doubling the value of the half-width of the left side (2*W_L) not modified by nucleation overvoltage [24, 35]. By applying this method and Eq. (10), the number of exchanged electrons was determined and is equal to 3.2 ± 0.1 with $W_{1/2}$ = 80 mV. The reduction of U(III) into U in LiCl-LiF is therefore a single step exchanging 3 electrons. Based on the work of Nourry et al. [43], square wave voltammetry can be used to determine the nucleation overvoltage η, using the following equation:

$$\eta = 2(W_L - W_R) \tag{11}$$

where W_L and W_R are respectively, the half-width of the left and on the right side of the peak. In our experiments, the nucleation overvoltage is equal to 123 mV.

For the soluble/soluble system the validity of Eq. (9) was verified in the frequency range 9–36 Hz, Eq. (10) was directly applied as the Gaussian curve is symmetric. The number of exchanged electrons was determined and equal to 1 ± 0.1 with $W_{1/2}$ = 250 mV. This confirms that this step involves the trans-

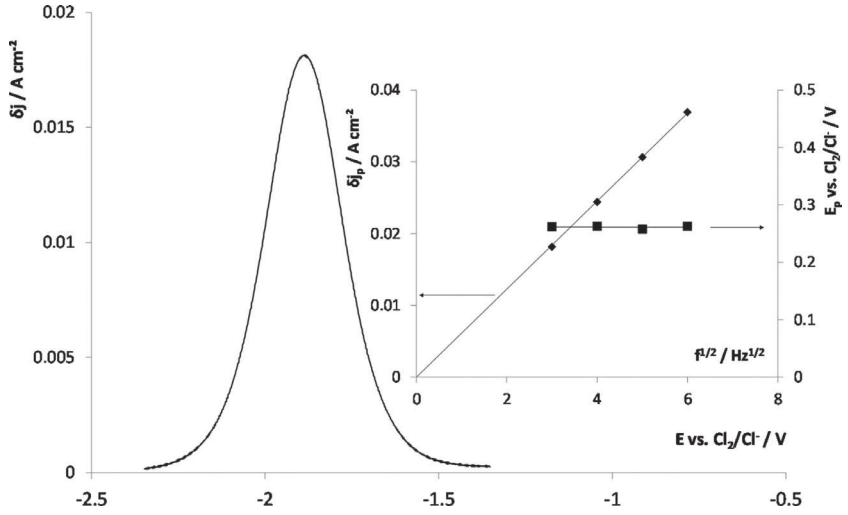

Fig. 5. Square wave voltammogram on W in LiCl-LiF-U(III) (0.039 mol kg^{-1}) system at 9 Hz and T = 823 K. Inset. Variation of the peak current density (left axis) and the oxidation peak potential (right axis) vs. the square root of frequency.

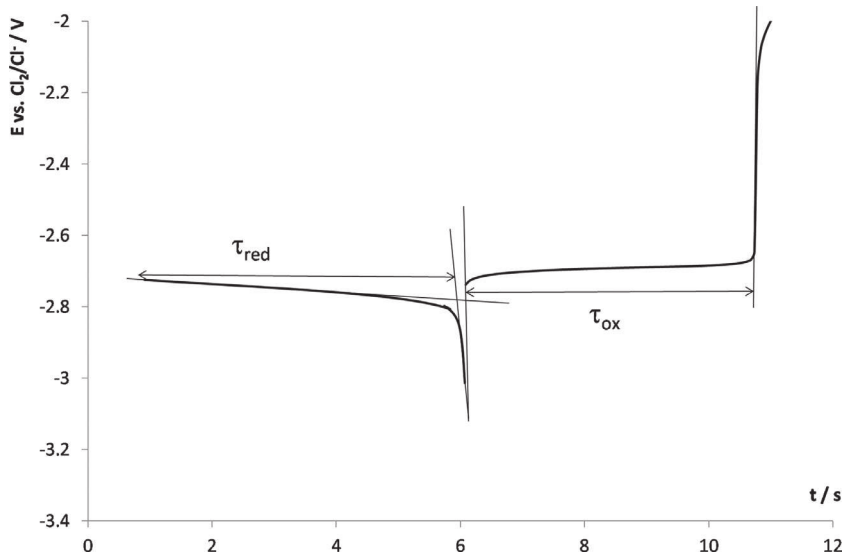

Fig. 6. Reversal chronopotentiogram on W in LiCl-LiF-U(III) (0.039 mol kg^{-1}) system at T = 823 K; applied current = ± 9.5 mA. Working El.: W; auxiliary el.: Mo; comparison el.: W.

fer of 1 electron and corresponds to the oxidation of the U(III) into U(IV).

3.1.3. Reverse chronopotentiogram

To confirm U deposition, a reversal chronopotentiogram was carried out at ± 9.5 mA and T = 832 K in LiCl-LiF-U(III) and the signal is plotted in Fig. 6. The anodic transition time τ_{ox} was found to be equal to the cathodic one τ_{red} with $\tau_{ox} = \tau_{red} = 4.7$ s and is typical of a solid phase deposition on the electrode [44].

3.1.4. Chronopotentiometry

Chronopotentiograms were obtained in LiCl-LiF-U(III) (0.039 mol kg^{-1}) at 823 K for different intensities (−10 to −18 mA). Fig. 7 shows a single plateau at −2.7 V vs Cl_2/Cl^-, corresponding to the reduction potential of U(III) observed in cyclic voltammetry. As described by the Sand's Law, the transition time τ decreases with the increase of the current density [45].

$$i\,\tau^{0.5} = 0.5\pi^{0.5}.n.F.D^{0.5}.C^{\circ} \quad (12)$$

where i is the current density applied (A cm^{-2}), τ the transition time (s).

According to the data plotted in Fig. 7:

$$i\,\tau^{0.5} = 0.095\ A.s^{0.5}.cm^{-2} \quad (13)$$

The Sand's law verification confirmed that the electrochemical reaction is controlled by the U(III) ions diffusion in the melt.

3.2. Determination of experimental physico-chemical data

3.2.1. U(III) diffusion coefficient

The U(III) diffusion coefficient was calculated in the 823–923 K temperature range, using the Berzins Delahay relationship. The numbers of exchanged electrons taken in account for the calculation was 3 according to the SWV. At T = 823 K and [U(III)] = 0.039 mol.kg^{-1}, the diffusion coefficient was found to be (2.0 ± 0.1) 10^{-5} cm^2 s^{-1} considering the U(III) reduction. With the Sand's law, U(III) diffusion coefficient was found to be (2.3 ± 0.1) 10^{-5} cm^2 s^{-1} at the same temperature. The results obtained are in the same order of magnitude than the previous ones determined by Serrano et al. with 5.6 10^{-5} cm^2.s-1 for U(III) in NaCl-KCl at 973 K and by Hoover et al. with 1.04 10^{-5} cm^2 s^{-1} in LiCl-KCl for U(III) [27,28].

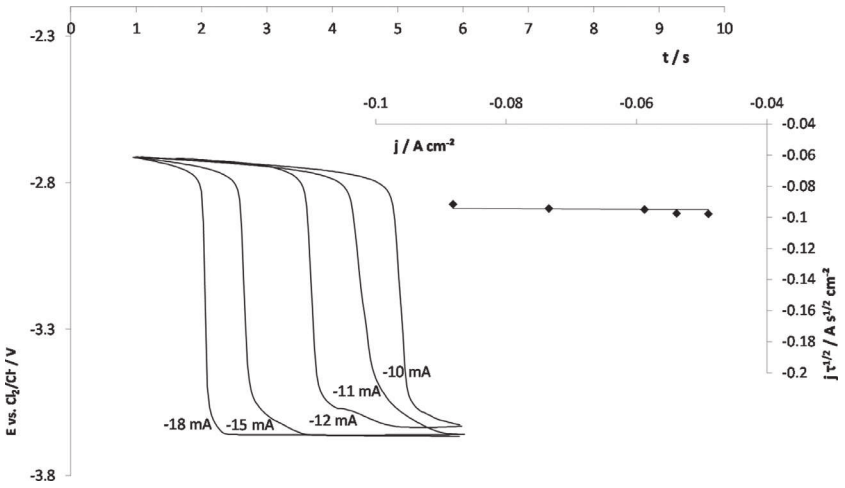

Fig. 7. Chronopotentiograms on W LiCl-LiF-U(III) (0.039 mol kg^{-1}) system from at −10, −11, −12, −15 and −18 mA and T = 823 K. Working El.: W; auxiliary el.: Mo; comparison el.: W. Inset. Variation of $i.\tau^{1/2}$ vs. the intensity at 823 K. Working el.: W; auxiliary el.: Mo; comparison el.: W.

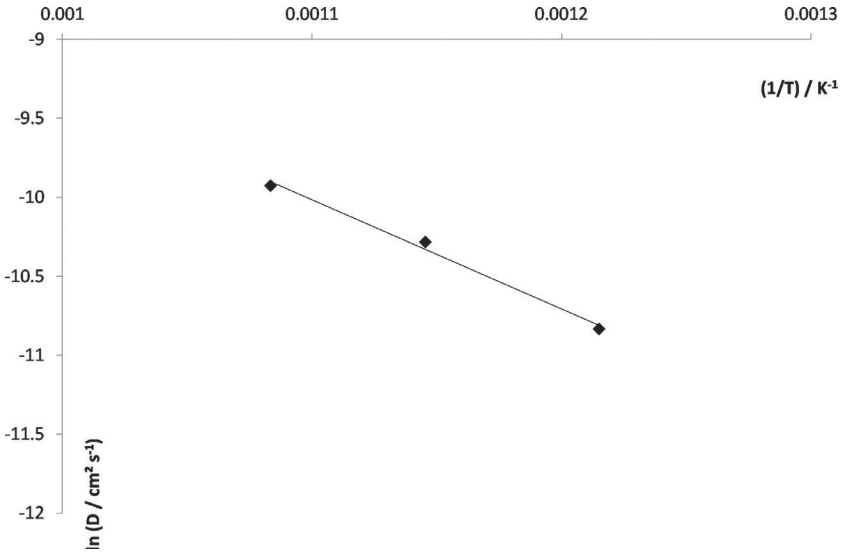

Fig. 8. Variation of the logarithm of the diffusion coefficient versus the inverse of the absolute temperature.

The U(III) diffusion coefficient was determined by cyclic voltammetry at three temperatures using the reduction of U (III) and the linear relationship between ln D and the inverse of the temperature (K) is plotted in Fig. 8. This Figure shows that the variation of the diffusion coefficient follows an Arrhenius' type law:

$$\ln D_{U(III)} = -2.42 - \frac{6907}{T} \quad (14)$$

The activation energy can be estimated to 57.4 kJ.mol^{-1}.

3.2.2. Apparent standard potentials

The apparent standard potentials of the U(IV)/U(III) and U(III)/U redox couple were measured in LiCl-LiF at 823 K and [U(III)] = 0.039 mol kg^{-1} ($x_{U(III)} = 1.42\ 10^{-3}$). To compare the electrochemical behavior of uranium in chloride and chloro-fluoride salts and the influence of fluoride complexation, voltammograms of uranium ions were carried out in LiCl-KCl salt at 823 K. Voltammograms presented on Fig. 9 were referred to the experimental Cl_2/Cl^- redox couple. in order to take into account the difference of activity of Cl^- in the two media, the potentials measured in LiCl-LiF versus the experimental reference were corrected by the term ΔE assuming an activity of Cl^- equal to its molar ratio, $a_{Cl^-} = 0.7$.

$$\text{For } T = 823\text{K},\ \Delta E = \frac{RT}{F}\ln\frac{1}{x_{Cl^-}} = 0.0253\ \text{V} \quad (16)$$

It can be pointed out that this value of ΔE is low.

The comparison of the two voltammograms obtained in LiCl-KCl-U(III) and LiCl-LiF-U(III) are shown in Fig. 9. It can be observed that (i) the presence of fluoride ions tends to form more stable complexes which are reduced at more negative potentials as frequently observed, and (ii) the difference between the potential of U(IV)/U(III) system in the two media is significantly more affected than the one of U(III)/U system.

The apparent standard potentials for both systems have been estimated in LiCl-LiF taking into account the activity of Cl^-:

v $E^{0'}_{U(IV)/U(III)}$, according to the theory of linear sweep voltammetry for a soluble-soluble system, can be expressed by [46]:

$$E^{0'}_{U(IV)/U(III)} = \frac{E^c_p + E^a_p}{2} \quad (17)$$

Where E^c_p and E^a_p are the experimental anodic and cathodic peaks potentials graphically determined on cyclic voltammograms (V) and $E^{0'}_{U(IV)/U(III)}$ is the apparent standard potential of the

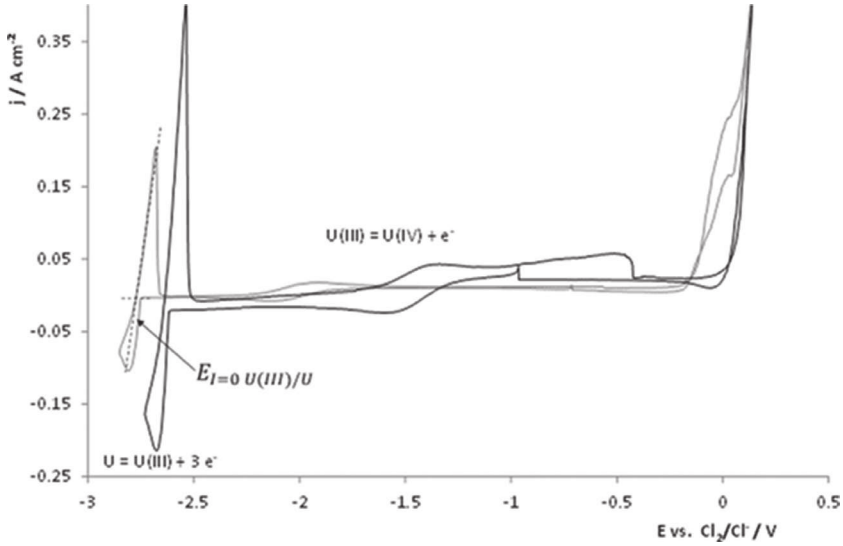

Fig. 9. Cyclic voltammograms on W of LiCl-LiF-U(III) (0.039 mol kg^{-1}) system (grey) and LiCl-KCl-U(III) (0.08 mol kg^{-1}) (black) at 100 mV s^{-1} and T = 823 K.

Table 1
Summary of $E^{0'}$ value for U(IV)/U(III) and U(III)/U couple in different molten salts.

Reference	Concentration of U(III)	Salt	T (°C)	$E^{0'}$ / V U(IV)/U(III)	$E^{0'}$ / V U(III)/U	$\Delta E^{0'}$ / V
Hoover [28]	1–10 wt%	LiCl-KCl	500	−1.448	−2.568	1.12
Masset [47]	9.87 10^{-5} mol cm^{-3}	LiCl-KCl	500	−1.428	−2.563	1.14
This studysssss	1.9 wt%	LiCl-KCl	550	−1.483	−2.496	1.01
This study	0.9 wt%	LiCl-LiF	550	−2.03	−2.59	0.6

U(IV)/U(III) couple (V). The obtained value at 823 K is $E^{0'}_{U(IV)/U(III)} = -2.02V$ vs Cl_2/Cl^-

The Eq. (18) connects the apparent standard potentials variation and the temperature in Kelvin for the U(IV)/U(III) system:

$$E^{0'}_{U(IV)/U(III)} = 1.4310^{-3}\,T - 3.2 \quad (18)$$

v $E^{0'}_{U(III)/U}$ can be expressed using the Nernst equation:

$$E_{I=0\ U(III)/U} = E^{0}_{U(III)/U} + \frac{RT}{nF}\ln\frac{a_{U(III)}}{a_U} \quad (19)$$

$$E_{I=0\ U(III)/U} = E^{0'}_{U(III)/U} + \frac{RT}{nF}\ln x_{U(III)} \quad (20)$$

Where $E_{I=0\ U(III)/U}$ is the Nernst potential (V) graphically determined as indicated on Fig. 10 and $E^{0'}_{U(III)/U}$ the apparent standard potential (V) of the U(III)/U couple. The obtained value at 823 K is: $E^{0'}_{U(III)/U^0} = -2.61$ V vs Cl_2/Cl^-

The relationship between the apparent standard potentials evolution and the temperature in Kelvin for the U(III)/U system is then:

$$E^{0'}_{U(III)/U} = 9.52\ 10^{-4}\,T - 3.4 \quad (21)$$

Table 1 compares the apparent standard potentials obtained in this study with values found in the literature for U(IV)/U(III) and U(III)/U systems. The presence of fluoride ions (LiF) causes a shift towards more negative values of the apparent standard potential of U(IV)/U(III) and U(III)/U couples. The potential shift is larger than 500 mV for the U(IV)/U(III) couple and less than 100 mV for U(III)/U depending on the bibliographic reference considered. The fluoride stabilizing effect is clearly more pronounced on the reduction potential of U(IV)/U(III) compared to U(III)/U. The potential difference between the 2 redox systems of uranium in presence of fluoride (0.6 V) is smaller than in pure chloride (> 1 V).

It is more difficult to discuss on apparent standard potentials for pure fluoride media since most of the authors worked with quasi-reference electrodes and cannot refer their electrochemical systems to fluorine gas evolution, as dissolution of metallic working electrode is observed first. Consequently, in order to compare our results in LiCl-LiF with pure fluoride salt, instead of listing apparent redox potentials, the difference between reduction peak potentials of U(IV)/U(III) and U(III)/U systems, ΔEpc, in LiF-CaF_2 and LiCl-LiF was collected in Table 2.

Table 2
Cathodic potential peak difference between U(III)/U reduction potential into LiF-CaF_2 and LiCl-LiF.

Reference	Concentration of U(III)	Salt	T (°C)	ΔE_{pc} (V)
Nourry [36]	2 wt%	LiF-CaF_2	810	0.58
Hamel [35]	0.76 wt%	LiF-CaF_2	810	0.53
This study	0.9 wt%	LiCl-LiF	550	0.65

The cathodic peak potential difference observed in chlorofluorides is close to the one observed in pure fluorides. These results show clearly that U(IV) is a stronger oxidant in chloride salt than in fluoride salt.

4. Conclusion

The electrochemical behavior of uranium ions was investigated in LiCl-LiF in the 823–923 K temperature range on a W electrode. In the experimental conditions, only U(III) was present in the molten salt with an excess of U metal in solution. In LiCl-LiF, U(III) is reduced into metal at around −2.59 V vs Cl_2/Cl^- and oxidized into U(IV) at around −2.03 V vs Cl_2/Cl^-:

Using different electroanalytical techniques such as cyclic voltammetry and chronopotentiometry, it was shown that both steps are diffusion controlled.

The value of diffusion coefficient for the U(III) in chloride and fluoride media are of the same order of magnitude. In the 823–

923 K temperature range the diffusion coefficient logarithm versus the temperature follows an Arrhenius type relationship.

The variation of the apparent standard potentials as a function of the temperature for the uranium systems have been evaluated.

This study showed the stabilizing effect of fluoride ions (LiF) affects the reduction potential peaks of U(IV)/U(III) and U(III)/U systems. The reduction potentials are shifted towards negative values. A comparison of the uranium electrochemical behavior in LiCl-LiF and LiCl-KCl salts clearly shows that the fluoride addition affects more the U(IV)/U(III) transition (500 mV shift) than the U(III)/U system (100 mV shift). The U(IV)/U(III) redox couple is a stronger oxidant in chloride salt than in chloro-fluoride or fluoride.

Future works will deal with the acquisition of similar data for Np, Pu and Am. The reduction potentials to metals of these transuranic elements species will be investigated in LiCl-LiF to improve knowledge about fluoride ions complexation effects. Difference in reduction potential between U and Pu species in LiCl-KCl and LiCl-LiF will be compared; electrolyses will be carried out below and above the plutonium metal melting point to assess the feasibility of using chloro-fluoride salts like LiCl-LiF for the group actinides recovery on inert electrodes.

Declaration of Competing Interest

The authors declare that they have no known competing financial interests or personal relationships that could have appeared to influence the work reported in this paper.

References

[1] M.F. Simpson, Developments of Spent Nuclear Fuel Pyroprocessing Technology at Idaho National Laboratory, 2012 Technical report, doi:10.2172/1044209.

[2] H. Lee, J.-.M. Hur, J.-.G. Kim, Dd-H. Ahn, Y.-.Z. Cho, S.-.W. Paek, Korean pyrochemical process R&D activities, Energy Procedia 7 (2011) 391.

[3] T. Koyama, M. Iizuka, Pyrochemical fuel cycle technologies for processing of spent nuclear fuels: developments in Japan, Reprocess. Recycl. Spent Nucl. Fuel. http://dx.doi.org/10.1016/B978-1-78242-212-9.00018-6.

[4] S.X Li, T.A Johnson, B.R Westphal, K.M Goff, R.W Benedict, Electro-refining Experience for Pyrochemical Reprocessing of Spent EBR-II Driver Fuel, INL/CON-05-00305, Global 2005.

[5] L. Burris, R.K. Steunenberg, W.E. Miller, The application of electrorefining for recovery and purification of fuel discharged from the Integral Fast Reactor, AIChE winter annual meeting, 1986 2-7 November.

[6] A.F. Laplace, J. Lacquement, J.L. Willit, R.A. Finch, G.A. Fletcher, M.A. Williamson, Electrodeposition of Uranium and Transuranics Metals (Pu) on Solid Cathode, Nucl. Technol. 163 (2008) 366.

[7] Z. Tomczuk, D.S. Poa, W.E. Miller, R.K. Steunenberg, Electrorefining of uranium and plutonium from liquid cadmium, American Nuclear Society winter meeting, 1985 10 november.

[8] Y. Sakamura, T. Murakami, K. Tada, S. Kitawaki, Electrowinning of U-Pu onto inert solid cathode in LiCl-KCl eutectic melts containing UCl_3 and $PuCl_3$, J. Nucl. Mater. 502 (2018) 270.

[9] M.A. Williamson, J.L. Willit, Pyroprocessing flowsheets for recycling used nuclear fuel, Nucl. Eng. Technol. 43 (2011) 329.

[10] J.L. Willit, W.E. Miller, J.E. Battles, Electrorefining of uranium and plutonium – a literature review, J. Nucl. Mater. 195 (1992) 229.

[11] T. Koyama, M. Iizuka, Y. Shoji, R. Fujita, H. Tanaka, T. Kobayashi, M. Tokiwai, An experimental study of molten salt electrorefining of uranium using solid iron cathode and liquid cadmium cathode for development of pyrometallurgical reprocessing, J. Nucl. Sci. Technol. 34 (1997) 384.

[12] M. Kurata, Y. Sakamura, T. Matsui, Thermodynamic quantities of actinides and rare earth elements in liquid bismuth and cadmium, J Alloys Compd 234 (1996) 83.

[13] J. Serp, M. Allibert, A. Le Terrier, R. Malmbeck, M. Ougier, J. Rebizant, J.-.P. Glatz, Electroseparation of Actinides from Lanthanides on Solid Aluminum Electrode in LiCl-KCl Eutectic Melts, J. Electrochem. Soc. 152 (2005) C167.

[14] K. Liu, Y.-L. Liu, Z.-F. Chai, W.-Q. Shia, Evaluation of the electroextractions of Ce and Nd from LiCl-KCl molten salt using liquid Ga electrode, J. Electro-chem. Soc. 164 (2017) D169.

[15] T. Murakami, S. Kitawaki, Y. Sakamura, M. Izuka, T. Nohira, H. Kofuji, Actinides separation from lanthanides using a liquid gallium electrode in LiCl-KCl melts, J. Radiochem. Sci. 16 (2016) 5.

[16] B.R. Westphal, J.C. Price, D. Vaden, R.W. Benedict, Engineering-scale distillation of cadmium for actinide recovery, J. Alloy. Compd. 444–445 (2007) 561.

[17] V. Smolenski, A. Novoselova, A. Osipenko, A. Maershin, Thermodynamics and separation factor of uranium from lanthanum in liquid eutectic gallium-indium alloy/molten salt system, Electrochim. Acta 145 (2014) 81.

[18] H.A. Wilhelm, Development of Uranium Metal Production in America, J. Chem. Educ. 37 (2) (1960) February.

[19] D.S. Poa, L. Burris, R.K. Steunenberg. and Z. Tomczuk, Laboratory-scale study of electrolytic reduction of uranium oxides, ANL-88-29.

[20] P.N. Haubenreich, J.R. Engel, Experience with the molten-salt reactor experiment, Nucl. Appl. Technol. 8 (2) (1970) 118.

[21] J. Serp, M. Allibert, O. Benes, S. Delpech, O. Feynberg, V. Ghetta, D. Heuer, D. Holcomb, V. Ignatiev, J.L. Kloosterman, L. Luzzi, E. Merle-Lucotte, J. Uhlir, R. Yoshioka, D. Zhimin, The molten salt reactor (MSR) in generation IV: overview and perspectives, Prog. Nucl. Energy 77 (2014) 308.

[22] T. Fukasawa, K. Hoshino, D. Watanabe, A. Sasahira, Application of fluoride volatility method to the spent fuel reprocessing, J. Nucl. Sci. Technol. 57 (2020) 49.

[23] D. Lambertin, J. Lacquement, S. Sanchez, G. Picard, Dismutation of divalent americium induced by the addition of fluoride anion to a LiCl–KCl eutectic at 743 K, Electrochem. Commun. 3 (2001) 519.

[24] D. Quaranta, L. Massot, M. Gibilaro, E. Mendes, J. Serp, P. Chamelot, Zirconium(IV) electrochemical behavior in molten LiF-NaF, Electrochim. Acta 265 (2018) 586.

[25] Y. Sakamura, Zirconium behavior in molten LiCl-KCl eutectic, J. Electrochem. Soc. 151 (2004) 187.

[26] L. Diaz, Développement d'un procédé d'électrolyse de terres rares (néodyme et dysprosium) en milieux de sels fondus PhD Thesis, University of Toulouse 3 – Paul Sabatier, Toulouse, 2018.

[27] K. Serrano, P. Taxil, Electrochemical reduction of trivalent uranium ions in molten chlorides, J. Appl. Electrochem. 29 (1999) 497.

[28] R.O. Hoover, M.R. Shaltry, S. Martin, K. Sridharan, S. Phongikaroon, Electrochemical studies and analysis of 1–10 wt% UCl_3 concentrations in molten LiCl–KCl eutectic, J. Nucl. Mater. 452 (2014) 389.

[29] O. Shirai, T. Iwai, Y. Suzuki, Y. Sakamura, H. Tanaka, Electrochemical behavior of actinide ions in LiCl-KCl eutectic melts, J. Alloy. Compd. 271–273 (1998) 685.

[30] G.Y. Kim, D. Yoon, S. Paek, S.H. Kim, T.J. Kim, D.H. Ahn, A study on the electrochemical deposition behavior of uranium ion in a LiCl-KCl molten salt on solid and liquid electrode, J. Electroanal. Chem. 682 (2012) 128.

[31] S.A. Kuznetsov, H. Hayashi, K. Minato, M. Gaune-Escard, Electrochemical behavior and some thermodynamic properties of UCl4 and UCl3 dissolved in a LiCl-KCl eutectic melt, J. Electrochem. Soc. 152 (4) (2005) C203.

[32] P. Masset, D. Bottomley, R. Konings, R. Malmbeck, A. Rodrigues, J. Serp, J.P. Glatz, Electrochemistry of uranium in molten LiCl-KCl eutectic, J. Electrochem. Soc. 152 (6) (2005) A1109.

[33] D. Rappleye, K. Teaford, M.F. Simpson, Investigation of the effects of uranium (III)-chloride concentration on voltammetry in molten LiCl-KCl eutectic with a glass sealed tungsten electrode, Electrochim. Acta 219 (2016) 721.

[34] B.P. Reddy, S. Vandarkuzhali, T. Subramanian, P. Venkatesh, Electrochemical studies on the redox mechanism of uranium chloride in molten LiCl-KCl eutectic, Electrochim. Acta 49 (15) (2004) 2471.

[35] C. Hamel, P. Chamelot, A. Laplace, E. Walle, O. Dugne, P. Taxil, Reduction process of uranium(IV) and uranium(III) in molten fluorides, Electrochim. Acta 52 (2007) 3995.

[36] C. Nourry, P. Soucek, L. Massot, R. Malmbeck, P. Chamelot, J.P. Glatz, Electrochemistry of uranium in molten LiF–CaF2, J. Nucl. Mater. 430 (2012) 58.

[37] G.M. Haarberg, E. Kvalheim, S. Rolseth, T. Murakami, S. Pietrzyk, S. Wang, Electro-deposition of iron from molten mixed chloride/fluoride electrolytes, ECS Trans. 3 (35) (2007) 341.

[38] Y. Norikawa, K. Yasuda, T. Nohira, Electrochemical Behavior of Ti(III) Ions in Molten LiF–LiCl: comparison with the Behavior in Molten KF–KCl, J. Electrochem. Soc. 167 (2020) 082502.

[39] Diaz L., Serp J., Serve G., Chamelot P., Gibilaro M., Massot L., Use of reverse chrono-potentiometry for the production of chemical elements in the metallic state or alloys thereof by electrolytic reduction in molten salt media, EP3431632.

[40] A.J. Bard, Electrochemistry: Principles, Methods and Applications, Wiley, New York, 1980.

[41] L. Ramaley, M.S. Krause, Theory of square wave voltammetry, Anal. Chem. 41 (1969) 1362.

[42] P. Chamelot, B. Lafage, P. Taxil, Using square-wave voltammetry to monitor molten alkaline fluoride baths for electrodeposition of niobium., Electrochim. Acta 43 (1998) 607.

[43] C. Nourry, L. Massot, P. Chamelot, P. Taxil, Data acquisition in thermodynamic and electrochemical reduction in a Gd(III)/Gd system in LiF–CaF_2 media, Electrochim. Acta 53 (2008) 2650.

[44] H.B. Herman, A.J. Bard, Cyclic chronopotentiometry. diffusion controlled electrode reaction of a single component system, Anal. Chem. 35 (1963) 1121.

[45] R.K. Jain, H.C. Gaur, B.J. Welch, Chronopotentiometry: a review of theoretical principles, J. Electroanal. Chem. Interfac. Electrochem. 79 (1977) 211.

[46] D.A.C. Brownson, C.E. Banks, Interpreting electrochemistry, The Handbook of Graphene Electrochemistry, 23, Springer, London, UK, 2014.

[47] P. Masset, R. Konings, R. Malmbeck, J. Serp, J.P. Glatz, Thermochemical properties of lanthanides (Ln = La, Nd) and actinides (An = U, Np, Pu, Am) in the molten LiCl–KCl eutectic, J. Nucl. Mater. 344 (2005) 173.